SCIENTIFIC REPORTS

OPEN

SUBJECT AREAS:
TWO-DIMENSIONAL MATERIALS
ELECTRONIC PROPERTIES AND DEVICES
ELECTRONIC DEVICES

Received
30 April 2014

Accepted
8 July 2014

Published
30 July 2014

Correspondence and requests for materials should be addressed to L.Q. (lqu@bit.edu.cn)

Functionalized Graphitic Carbon Nitride for Metal-free, Flexible and Rewritable Nonvolatile Memory Device via Direct Laser-Writing

Fei Zhao[1], Huhu Cheng[1], Yue Hu[1], Long Song[1], Zhipan Zhang[1], Lan Jiang[2] & Liangti Qu[1]

[1]Key Laboratory of Cluster Science, Ministry of Education, School of Chemistry, Beijing Institute of Technology, Beijing 100081, China, [2]Laser Micro-/Nano-Fabrication Laboratory, School of Mechanical Engineering, Beijing Institute of Technology, Beijing 100081, China.

Graphitic carbon nitride nanosheet (g-C_3N_4-NS) has layered structure similar with graphene nanosheet and presents unusual physicochemical properties due to the s-triazine fragments. But their electronic and electrochemical applications are limited by the relatively poor conductivity. The current work provides the first example that atomically thick g-C_3N_4-NSs are the ideal candidate as the active insulator layer with tunable conductivity for achieving the high performance memory devices with electrical bistability. Unlike in conventional memory diodes, the g-C_3N_4-NSs based devices combined with graphene layer electrodes are flexible, metal-free and low cost. The functionalized g-C_3N_4-NSs exhibit desirable dispersibility and dielectricity which support the all-solution fabrication and high performance of the memory diodes. Moreover, the flexible memory diodes are conveniently fabricated through the fast laser writing process on graphene oxide/g-C_3N_4-NSs/graphene oxide thin film. The obtained devices not only have the nonvolatile electrical bistability with great retention and endurance, but also show the rewritable memory effect with a reliable ON/OFF ratio of up to 10^5, which is the highest among all the metal-free flexible memory diodes reported so far, and even higher than those of metal-containing devices.

Two-dimensional (2D) materials have attracted considerable attention owing to their unique properties derived from the quantum confinement effect in plane[1–5]. In particular, graphitic carbon nitride (g-C_3N_4), generally presenting a graphite-like layered structure[6,7], has proved its importance in photo-/electro-catalysis and bioimaging associated with its tunable band-gap, large surface area and biocompatibility[8–10]. However, g-C_3N_4 possesses a poor electronic conductivity attributed to the band gap of about 2.6 eV and the contact resistance between the nanosheets, which limits its application to a large extent[9–12]. Nevertheless, the dielectric characteristic is essential for specific devices such as memory diodes[13], in which the dielectric function of the active layer is highly expected since it could significantly lower the current level at "OFF" state to improve the ON/OFF ratio and thus reduce the risk of misreading during the read operation[14].

Up to now, memory diodes have been studied intensively as a leading candidate for nonvolatile memory and reconfigurable logic applications typically based on the sandwich metal/insulator/metal (MIM) structure[15–20], in which a series of metallic oxides (e.g. ZnO, GeO_x, Al_xO_y, TiO_2, MoS_2 etc.) active layers serve as the insulator[21–26], and the ultrapure metals (e.g. Al, Cu, Au, Ag, Pt etc.) or indium tin oxide (ITO) are the widely used electrodes[27–32]. However, these metal-containing materials suffered from the shortcomings of rigidity, high cost and/or limited availability in the earth[33]. Consequently, metal-free 2D materials with unique electric or dielectric property have been introduced into flexible, economical and eco-friendly memory diodes. For instance, some promising memory diodes based on graphene oxide (GO) film as the active insulator layer have been presented[34,35]. However, the device reliability is an inevitable issue due to the unstability of active oxygen functional groups on GO[36,37]. Meanwhile, GO layers have to be coupled with specific metal electrodes to achieve the rewritable function and enhance the ON/OFF ratio[38]. Compared with GO, g-C_3N_4 possesses not only the improved stability under electrical field or light pulse, but also provides large numbers of lone-pair electrons that helpful for its electronic coupling with nonmetal electrodes[8,13], which therefore holds the great promise as active layer for the

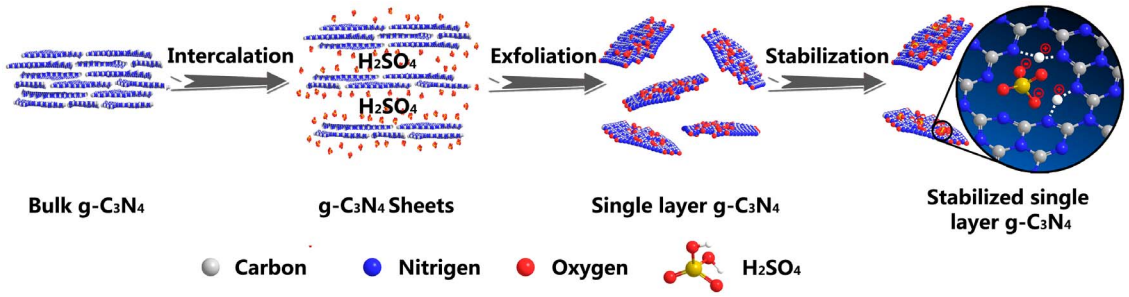

Figure 1 | Preparation process of g-C_3N_4 nanosheets. Schematic illustration of experimental procedure from bulk g-C_3N_4 to g-C_3N_4-NSs.

construction of high-performance memory devices. As far as we know, however, there was still no report on the memory devices based on the g-C_3N_4 sheets.

Flexible devices present significant advantage for future electronic applications such as portable and wearable electronics. In particular, metal-free flexible memories have merits such as low-cost, foldable and ambient temperature manufacturing. However, one of the most important challenge for fabrication of metal-free flexible memory diodes is that the devices should be supported on nonmetal and bendable electrodes. In this regard, graphene is considered to be a proper substitute owing to its desirable carrier mobility, chemical stability and flexibility[33]. Compared with the graphene obtained by micromechanical cleavage[39], epitaxial growth[40], and solvothermal synthesis[41], GO as the initial material is more compatible with the large-scale solution processing fabrication of memory device. Although the reductions of GO to graphene (also called rGO) are often facing the challenges of high temperature, toxic reagent and/or inefficiency[33], the recently-developed laser irradiation presents a facile, fast and efficient approach for region-confined reduction of GO to the transparent and flexible rGO film as demonstrated by us and other groups[42–45], which provides the new means for electrode fabrication.

Herein, we develop an all-solution processable strategy for metal-free, flexible and rewritable nonvolatile memory device based on the rationally assembled g-C_3N_4 nanosheets (g-C_3N_4-NSs) as the active insulator layer and direct laser writing graphene as electrodes. The as-fabricated memory device shows the nonvolatile electrical bistability and rewritable memory effect with a reliable ON/OFF ratio of up to 10^5, which, to the best of our knowledge, is comparable to those of metal-based memory devices and better than any other metal-free flexible memory diodes reported previously (Table S1). This fabrication procedure also provides a low-cost, environment-friendly, fast and facile manufacturing process for various electronics beyond high-performance memory devices demonstrated in this study.

Results

Morphology and chemical states of g-C_3N_4-NSs. The bulk g-C_3N_4 was treated by concentrated acid and oxidant to achieve the intercalation and exfoliation as shown in Fig. 1. The obtained g-C_3N_4-NSs presented the size ranging from 20 nm to 50 nm (Fig. 2A and B) and a typical topographic height of about 0.4 nm (Fig. 2C and D), which were significantly smaller than those of the intercalated g-C_3N_4 (Fig. S1 and S2), suggesting that the g-C_3N_4 were exfoliated to atomically thick sheets rather than multi-layers[9,10]. Note that the thickness of the single layer g-C_3N_4-NSs was slightly larger than the theoretical value of 0.326 nm[1], most probably due to the presence of functional groups (Fig. 2E).

The X-ray photoelectron spectroscopy (XPS) provided direct evidence of chemical state for g-C_3N_4-NSs. As shown in Fig. 2E, the

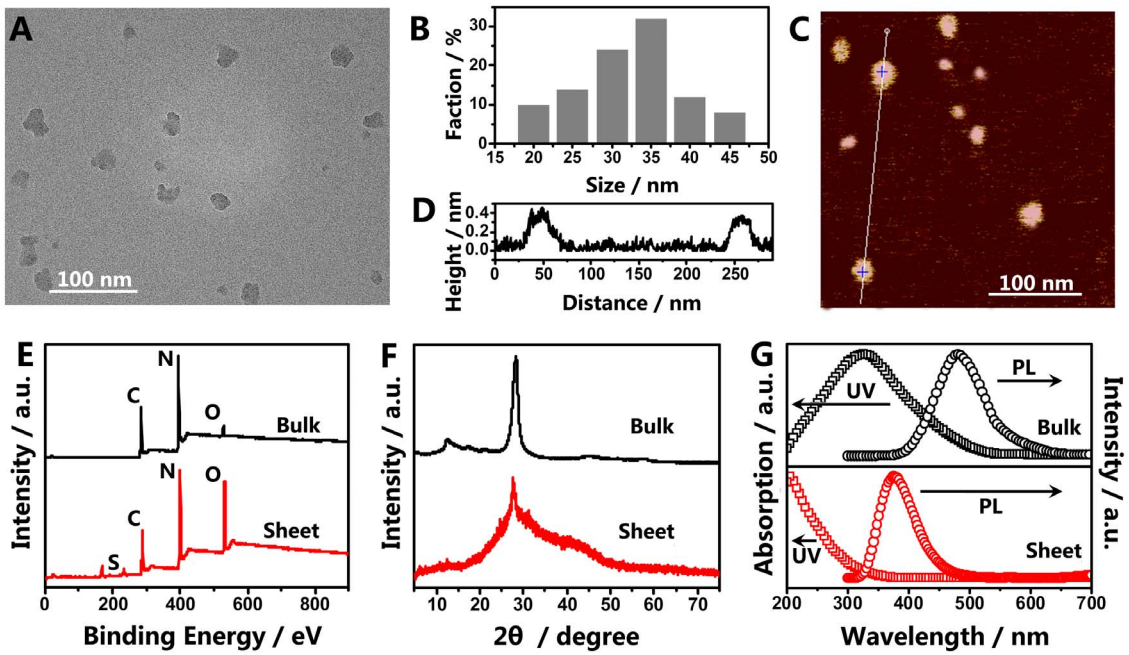

Figure 2 | Functional g-C_3N_4-NSs. (A) TEM image and (B) the size distribution of as-prepared g-C_3N_4-NSs, (C) AFM image of the g-C_3N_4-NSs on a Si substrate and (D) the height profile along the lines in (C). (E) XPS spectra, (F) XRD patterns, (G) UV-vis absorption and PL spectra of the original bulk g-C_3N_4 and g-C_3N_4-NSs, respectively.

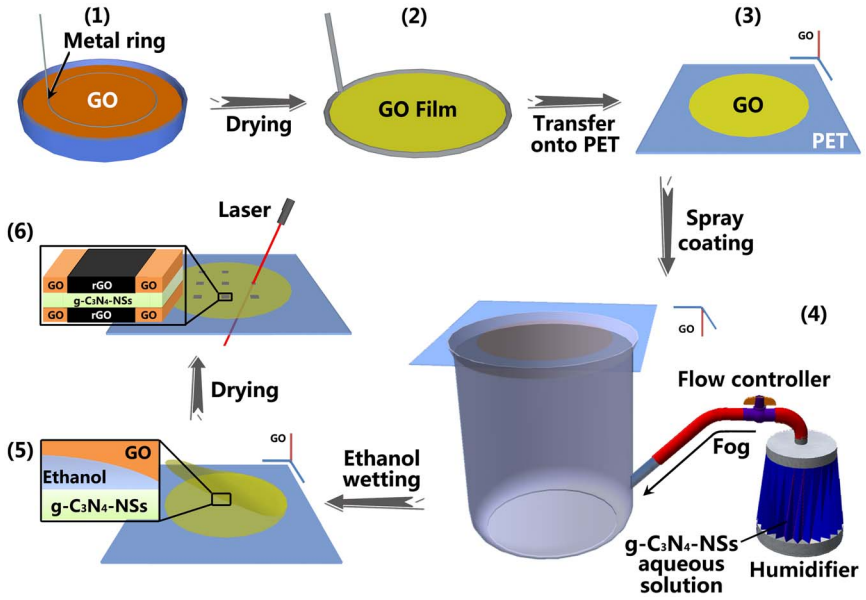

Figure 3 | Fabrication of the memory device. Schematic illustration of the experimental procedure for fabrication of the memory device.

g-C_3N_4-NSs exhibited C 1s, N 1s, O 1s, S 2s and S 2p signals with a N/C atomic ratio of 1.21, close to the ideal g-C_3N_4 composition (N/C = 1.33)[1] and almost the same to that of its parent bulk g-C_3N_4 sample (N/C = 1.23), suggesting that the chemical composition and the coordination of carbon and nitrogen in g-C_3N_4-NSs were retained. But a much higher O peak was observed for the as-prepared g-C_3N_4-NSs than bulk g-C_3N_4, indicating the possible occurrence of oxidation during sample preparation. High resolution C 1s spectrum (Fig. S3A) revealed the existence of C-OH (285.6 eV), C=O (288.8 eV) and O-C=O (289.3 eV), C-NH (286.8 eV), C=N and C-N bonds of sp^2 hybridized carbon in tri-s-triazine rings (287.4 and 288.1 eV)[9,47], which, in consistence with the analysis of N 1s and O1s XPS (Fig. S3B and C), confirmed that the g-C_3N_4-NSs had the intrinsic structure of g-C_3N_4 with oxygen functional groups[47]. In addition, the high resolution S 2p peak (Fig. S3D) verified the absence of S-C and S-N bonds, suggesting that there was no covalent bonding between the H_2SO_4 molecules and g-C_3N_4-NSs[48].

X-ray diffraction patterns (XRD) of as-prepared g-C_3N_4-NSs presented one predominant (002) peak at ca. 26.6° similar with their bulk counterparts, while the low-angle reflection peak of bulk g-C_3N_4 located at 13.3° disappeared for the g-C_3N_4-NSs (Fig. 2F)[1,9,46]. With respect to the (002) peak stemmed from the periodic stacking of layer structure[1,9], a slight shift from 27.6° for bulk g-C_3N_4 to 26.6° for g-C_3N_4-NSs occurred, suggesting a similar intrinsic crystal structure as the bulk one but with an increased interlayer spacing due to the presence of functional groups on the surface of g-C_3N_4-NSs. The peak located at 13.3° was originated from the in-planar repeat period of tri-s-triazine units with small tilt angularity in bulk g-C_3N_4[1], which was absent for g-C_3N_4-NSs due to the decreased planar size and structural defects[9,46], as observed from TEM and XPS mentioned above.

The normalized ultraviolet visible (UV-vis) absorption spectra and photoluminescence (PL) spectra showed an obvious blue shift of the g-C_3N_4-NSs with respect to the bulk g-C_3N_4, suggesting that the band gap of g-C_3N_4 was enlarged (Fig. 2G)[9,46]. The band gaps of g-C_3N_4-NSs and its parent g-C_3N_4 were determined from the $(ahv)^2$ versus photon-energy plots (Fig. S4) to be about 3.85 eV and 2.61 eV, respectively. Compared with bulk g-C_3N_4, the broadened energy gap of g-C_3N_4-NSs suggested the enhanced dielectricity[33]. It was speculated that this phenomenon was attributed to in-plane electron-confined effect of small-sized 2D nanostructure[48], electron-withdrawing effect of oxygen-containing groups[49] and electron-trapping effect of structural defects[13].

Sandwich structure of rGO/g-C_3N_4-NSs/rGO thin film. Based on the dielectricity, desirable dispersibility, and abundant functional groups, the g-C_3N_4-NSs present the great potential as active insulator layer for memory diode. For this purpose, we developed a new solution processable approach for constructing the sandwich-structured memory diodes with the graphene electrodes. As schematically shown in Fig. 3, a metal ring of stannum wire was employed as the support to prepare GO thin films from 1.5 mg/mL GO solution (step 1 to 2 and Fig. S5)[50], which was then transferred onto a poly(ethylene terephthalate) (PET) substrate (step 3) by wet-transferring process[33]. The formed GO film was crackless with some wrinkles (Fig. S6) like the common graphen-based film[36,51]. The g-C_3N_4-NSs film was formed on GO layer through the sprayed fog of g-C_3N_4-NSs aqueous solution in virtue of a commercial humidifier (step 4). It is worth mentioning that, due to the good hygroscopicity of GO[44], the GO film would allow the compact contact between g-C_3N_4-NSs fog and GO layer. As a result, a seamless g-C_3N_4-NSs layer was formed and its thickness was limited by the negligible hygroscopicity of g-C_3N_4-NSs surface. (Fig. 4A). Then another GO film was rapidly covered on the g-C_3N_4-NSs layer, where a droplet of ethanol was absorbed in advance (step 5). After dried in warm air of about 60°C for 30 min, the uniform GO/g-C_3N_4-NSs/GO complex film was obtained, which was subsequentnly converted into the rGO/g-C_3N_4-NSs/rGO (insert of step 6 and Fig. 4B) by direct laser scanning within the confined region (step 6). In this way, both the top and bottom GO layers were reduced simultaneously, while the g-C_3N_4-NSs layer remained laser-transparent. The laser induced rGO electrodes were 3 mm × 1 mm in size. Notably, because of high water swelling rate of GO[44], these wrinkles on GO film to some extent protected it from cracking during the absorption of g-C_3N_4-NSs fog. On the other hand, compact g-C_3N_4-NSs layer was spontaneously formed between the surfaces of GO films once dried (Fig. 4C) due to their interface compatibility. The whole thickness of the sandwich structure was ca. 150 nm (Fig. 4D), where g-C_3N_4-NSs layer was only ca. 30 nm (Fig. S7). Upon the laser irradiation, GO was highly reduced (Fig. S8), while the g-C_3N_4-NSs layer maintained its morphology and composition (Fig. S9).

Reversible and reliable electrical bistability of g-C_3N_4-NSs based device. The current-voltage (*I-V*) characteristics of the device presented the typical memory effect (Fig. 5A). Initially, the current gradually increased with a negative increase of applied voltage (stage

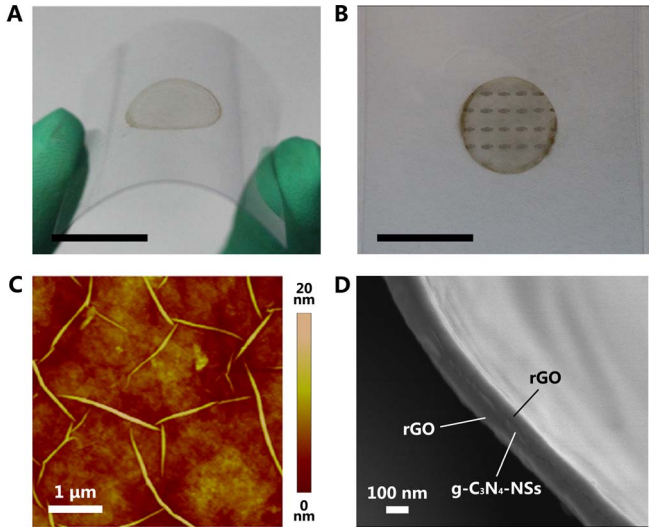

Figure 4 | Characterization of the memory device. Photographs of (A) flexible GO/g-C_3N_4-NSs/GO film on a PET substrate, and (B) the memory devices fabricated by laser irradiation with configuration of rGO/g-C_3N_4-NSs/rGO. Scale bars: B and C, 2 cm. (C) AFM image of the surface of g-C_3N_4-NSs film coated on GO film. (D) Cross-section SEM image of the rGO/g-C_3N_4-NSs/rGO sandwich structure.

I). When the voltage approached the switching threshold of ca. −4.87 V (stage II), the current abruptly jumped from 7.85×10^{-10} to 4.34×10^{-5} A, indicating the device achieved the write process in the data storage operation by resistive switching from a high resistance state (HRS, i.e., OFF state) to a low resistance state (LRS, i.e., ON state). The current ON/OFF ratio was about 10^5. After the resistive switching, the device retained the ON state during the subsequent sweep (stage III, IV and V). Even if the power was turned off, it still preserved the nonvolatile nature. Impressively, the OFF state could be recovered when the voltage approached the positive switching threshold of ca. 4.01 V (stage VI), implying the function of erasable data storage. Moreover, stage VII and VIII exhibited stable OFF state similar to that of stage I, indicating that the erase process in the data storage operation was achievable in this device.

The ON/OFF ratio determines the misreading probability during the practical operations of the memory devices. Fig. 5B presents an overall comparison of the previously reported flexible sandwich-structure memory diodes with the current work. As can be seen, based on the metal-containing electrodes, and metal oxides or other insulator layers (blue and green bars), few of the devices could reach the high ON/OFF ratios of ca. 10^5–10^6 with rewritable feature. In contrast, for the metal-free devices fabricated previously (red bars), the achieved ON/OFF ratio is only ca. 10^3 at best. As a result, only 8% the studies were focused on the metal-free memory devices (inset of Fig. 5), indicating the extreme challenge for development of the memory diodes with high ON/OFF ratio and outstanding characteristics of flexibility and rewritability. Herein, the developed rGO/g-C_3N_4-NS/rGO device exhibits the record high ON/OFF ratio for metal-free, flexible and rewritable memory diodes so far.

To investigate the reliability of the memory device, the retention, endurance and flexibility tests were conducted in the ON and OFF states. Fig. 6A showed the retention property of the device for a test period of 5000 s under ambient conditions. This device maintained the ON/OFF ratio at the level of ca. 10^5 without significant variation at a bias of −1 V, indicating the great retention ability. The endurance performance was demonstrated with steady operation for 50 cycles and the resistance values were read out at −1 V (Fig. 6B). Although the current values showed slight fluctuations, the ON/OFF ratio was retained. Obviously, the device exhibited excellent

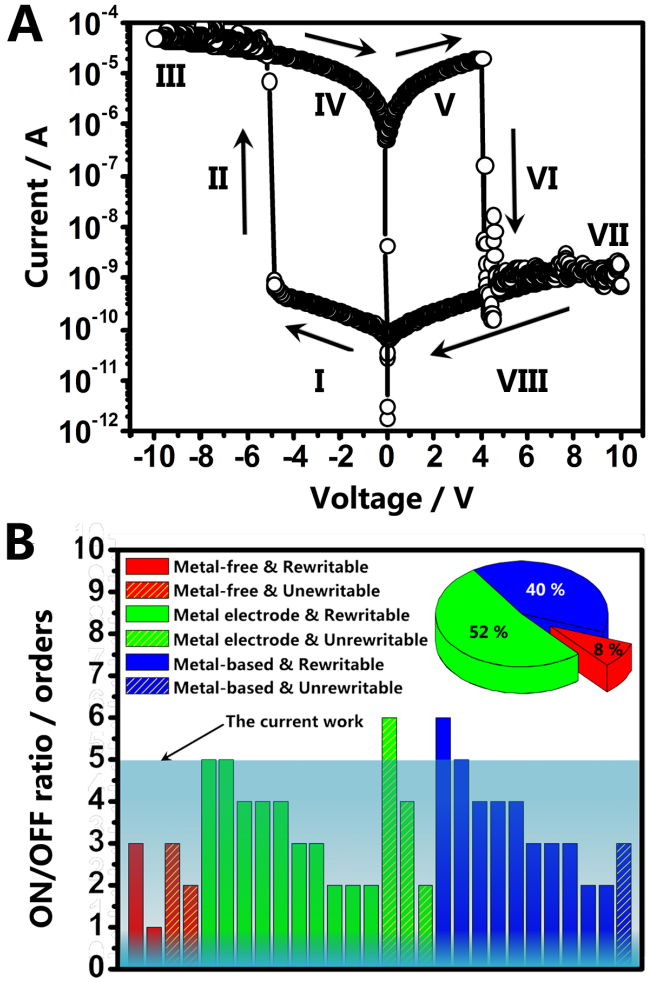

Figure 5 | Performance of the memory device. (A) Typical I-V curve of a rGO/g-C_3N_4-NS/rGO device with arrows showing the voltage sweep direction. (B) The ON/OFF ratios of flexible memory diodes reported previously with nonmetal electrodes and insulator layer (Metal-free), metal electrode and nonmetal insulator layer (Metal electrode), metal-containing electrodes and insulator layer (Metal-based) compared with that of rGO/g-C_3N_4-NSs/rGO in current work. Inset: the pie chart of the percentage for each kind of flexible and rewritable memory diodes. This figure is derived from Table S1 in Supporting Information.

sustainability that might be attributed to the stability of g-C_3N_4-NSs insulator layer, the electrical inertia of the rGO electrode and the compact contact between them.

The flexibility test was performed by the repetitive bending and relaxing of this device with a bent radius of 8 mm for 1000 times (Fig. S10). It was observed that there was no electrical degradation at either ON or OFF state at the reading voltage of −1 V (Fig. 6C). Since the g-C_3N_4-NSs were single layered 2D material, whose self-formed orientation and relative slip caused by stress enabled the strain tolerance, and the graphene films could keep its resistance stable in both the longitude and transverse direction under stretching[52], the outstanding mechanical endurance of the fabricated device was well deserved.

Discussion

To improve the dispersability and tune the dielectric property of g-C_3N_4, we have prepared the functionalized g-C_3N_4-NSs as schematically shown in Fig. 1, which have stoichiometric N/C atomic ratio and exist in the form of single atomic layers. Briefly, bulk g-C_3N_4 was firstly intercalated by sulphuric acid (H_2SO_4). The formed multilayer

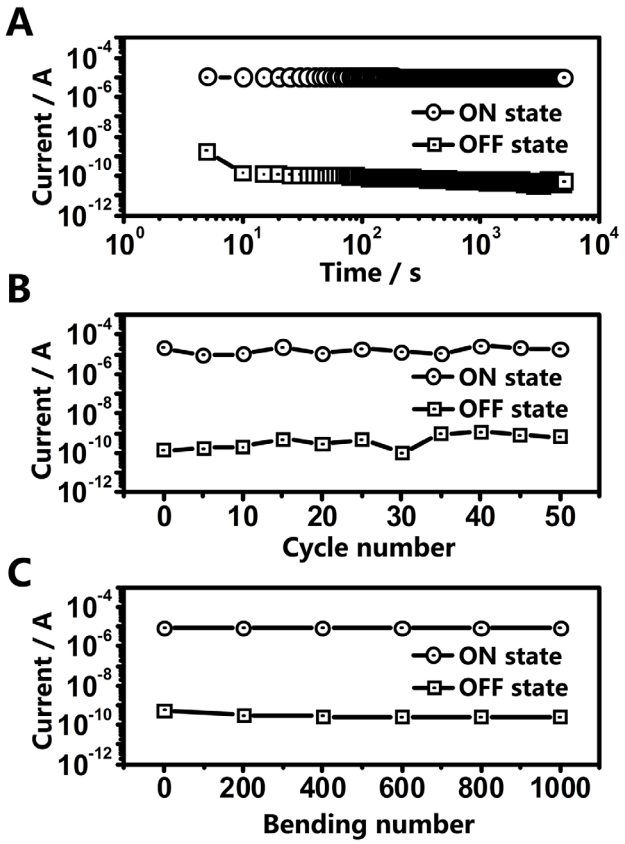

Figure 6 | Reliability of the memory device. (A) Retention test, (B) Endurance performance and (C) Bending experiment of the memory device at a reading voltage of −1 V under ambient condition.

fragments were further exfoliated by oxidation. Subsequently, the purified g-C_3N_4-NSs were protonized by dilute H_2SO_4 to avoid the reaggregation[53]. Finally, the excess acid was removed completely by adequate dialysis. By curve fitting analysis of the XPS results (Fig. 2E), we can find the existence of sulfate ion, which implying that the g-C_3N_4-NSs were protonized as shown in Fig. 1. These charged ions could be the defects in the dielectric layer under applied voltage, and thus they are helpful for the electrical bistability. Moreover, there are plenty of wrinkles on the obtained GO film (Fig. S6), and these wrinkles are retained in the preparation of tri-layered device (Fig. 4E). The electrons are tending to accumulate around the peaks of the wrinkles, and the tunnelling will take place under a high level applied voltage[53]. Accordingly, it is highly probable that the obtained devices are enabled to provide electrical bistability based on a tunneling process.

As we have seen, the assembled g-C_3N_4-NSs film has exhibited the electrical stability for the high-performance memory device. For the common MIM devices, the memory effect is believed to be caused by the formation of metal filaments arising from the diffusion of metal electrodes under applied voltage, which largely increases the risk of insulator layer invalidation caused by electrothermal effect of high level ON state current[54]. Herein, "non-diffusible" rGO electrodes enabled the improved reliability of metal-free devices. Furthermore, the contact of g-C_3N_4-NSs and rGO benefited from the strong π - π interaction between these 2D structures[39] instead of Schottky contact in MIM devices[55], which also favored the unrestricted charge transference[13].

To propose a possible mechanism of high device performance with advantageous g-C_3N_4-NSs as active layer, the experimental data were fitted with classical models. In low-bias region, the plot of ln (I) vs. $V^{1/2}$ from 0 to −0.71 V was fitted to a straight line with Equation S1[56], suggesting that the conduction mechanism probably arose from the thermionic emission (Fig. S11)[13]. With the continuous increase of voltage, the conductive behavior changed (Figuer S12) while the device was maintained in OFF state. Fig. S13 showed the ln (I/V^2) vs. I/V plot to support the resistive switching based on Fowler-Nordheim (F-N) tunneling model[57], where the constant K_d (opposite number of slope of the fitting curve, Equation S4) was measured to be 320.31, implying that the ON state achieved by tunneling current with a reasonable barrier height of ca. 0.8 eV calculated from Equation S5. Therefore, the switching of our device can be attributed to the space charges accumulated at the wrinkles and interfaces between rGO and g-C_3N_4-NSs. When the traps were filled with electrons beyond −4.35 V, the tunneling process was occurred and resulted the switching. In addition, the devices fabricated with cross-bar model and without active layer further confirm that the memory effect in this work is only attributed to g-C_3N_4-NSs for active insulator layer (Fig. S14 to S16).

In conclusion, we develop an all-solution processsable strategy for metal-free, flexible and rewritable nonvolatile memory device based on the rationally assembled g-C_3N_4-NSs as the insulator layer and direct laser writing graphene as electrodes. The as-prepared g-C_3N_4-NSs have atomic thickness, excellent dispersability, desirable stability and considerable dielectricity. Accordingly, the fabricated memory device shows the nonvolatile electrical bistability and rewritable memory effect with a reliable ON/OFF ratio of up to 10^5, better than all the metal-free flexible memory diodes reported previously. This device fabrication procedure also provides a low-cost, fast and facile process for manufacturing various electronics beyond high performance memory devices demonstrated in this study.

Methods

Preparation of bulk g-C_3N_4. The bulk g-C_3N_4 was prepared by low temperature thermal condensation of analytical grade melamine. Generally, 10 g obtained powder were then put into a 20 mL alumina crucible, which was subsequently placed in the central region of a quartz tube furnace for heat treatment. The g-C_3N_4 was obtained after heating melamine at a 600°C for 2 h. After cooling to room temperature, the yellow product was taken out and ground into fine powers in the agate mortar.

Preparation of g-C_3N_4-NSs. 2 g g-C_3N_4 powders and 100 mL sulphuric acid (H_2SO_4) were added in a 500 mL beaker with vigorous stirring for 24 h. Whereafter, 1 g sodium nitrate ($NaNO_3$) and 11 g potassium permanganate ($KMnO_4$) were slowly added into the beaker and stirred for 10 h under ambient condition. The product was diluted to 300 mL by deionized water (140 mL) and 30 wt% hydrogen peroxide (60 mL). Finally, the white product was obtained by dialyze the diluted solution for 3 days.

Along with the method reported previously, the typical stabilizing process could be undertaken by ultrasonic treatment of 1 g exfoliated g-C_3N_4 with 100 mL dilute H_2SO_4 (~25 wt%) for 3 h at room temperature. The obtained white solution was purified by DI water dialysis until neutral condition to remove the excess H_2SO_4, and dried at 50°C in warm air.

Preparation of GO film. Grephene oxide (GO) suspension is prepared by modified Hummers method as we have reported[44]. GO films were produced by direct drying the foam of GO captured with metal rings[52].

Fabrication of flexible metal-free memory devices. The flexible memory devices were fabricated on the PET subtract. Firstly, a GO film was transfered on PET subtract. Then the GO/PET film was covered on a beaker which is filled with g-C_3N_4-NSs fog (or intercalated g-C_3N_4 and as exfoliated g-C_3N_4 in controlled experiment) for 1 min, where the fog was produced by 0.3 mg/mL aqueous solution of g-C_3N_4-NSs with commercial humidifier. The absorption step was controlled by g-C_3N_4-NSs fog flow with a flux of ca. 5 mL/min for 2 min. Herein, this step should be repeated 3 times to guarantee that the GO film was completely covered by g-C_3N_4-NSs. Another GO film was then transferred onto the surface of the g-C_3N_4-NSs film which was absorbed a droplet of ethanol in advance. Finally, a 458 nm laser with a power of 3 W was employed to write the devices by reducing the GO layers of GO/g-C_3N_4-NSs/GO structure.

Characterization. The morphology of the samples was examined by scanning electron microscope (SEM, JSM-7001F), transmission electron microscopy (TEM, JEM-2010 electron microscopy), and atomic force microscopy (AFM, Veeco D3100 atomic force microscope). X-ray photoelectron spectroscopy (XPS) data were recorded on an ESCALAB 250 photoelectron spectrometer (ThemoFisher Scientific) with Al Kα (1486.6 eV). X-ray diffraction (XRD) patterns were obtained by using a

Netherlands 1,710 diffractometer with a Cu Kα irradiation source (λ = 1.54 Å). The UV-Vis absorption and the photoluminescence (PL) spectra were measured with a 5300pc spectrophotometer and a SPEX flourolog-3 fluorimeter. The *I-V* curves were performed by using a Keithley 6300 semiconductor parameter analyzer under ambient conditions.

1. Wang, X. C. *et al.* A metal-free polymeric photocatalyst for hydrogen production from water under visible light. *Nat. Mater.* **8**, 76–80 (2009).
2. Geim, A. K. & Novoselov, K. S. The rise of graphene. *Nat. Mater.* **6**, 183–191 (2007).
3. Colson, J. W. & Dichtel, W. R. Rationally synthesized two-dimensional polymers. *Nat. Chem.* **5**, 453–465 (2013).
4. Du, Y. P. *et al.* A general method for the large-scale synthesis of uniform ultrathin metal sulphide nanocrystals. *Nat. Commun.* **3**, 1177 (2012).
5. Huang, X. *et al.* Solution-phase epitaxial growth of noble metal nanostructures on dispersible single-layer molybdenum disulfide nanosheets. *Nat. Commun.* **4**, 1444–1449 (2013).
6. Thomas, A. *et al.* Graphitic carbon nitride materials: variation of structure and morphology and their use as metal-free catalysts. *J. Mater. Chem.* **18**, 4893–4896 (2008).
7. Groenewolt, M. & Antonietti, M. Synthesis of g-C_3N_4 Nanoparticles in Mesoporous Silica Host Matrices. *Adv. Mater.* **17**, 1789–1792 (2005).
8. Du, A. *et al.* Hybrid Graphene and Graphitic Carbon Nitride Nanocomposite: Gap Opening, Interfacial Charge Transfer and Enhanced Visible Light Response. *J. Am. Chem. Soc.* **134**, 4393–4397 (2012).
9. Niu, P., Zhang, L., Liu, G. & Cheng, H. M. Graphene-Like Carbon Nitride Nanosheets for Improved Photocatalytic Activities. *Adv. Funct. Mater.* **22**, 4763–4770 (2012).
10. Zhang, X. *et al.* Enhanced photoresponsive ultrathin graphitic-phase C_3N_4 nanosheets for bioimaging. *J. Am. Chem. Soc.* **135**, 18–21 (2012).
11. Su, F. *et al.* Mpg-C_3N_4-catalyzed selective oxidation of alcohols using O_2 and visible light. *J. Am. Chem. Soc.* **132**, 16299–16301 (2010).
12. Wang, Y., Wang, X. & Antonietti, M. Polymeric graphitic carbon nitride as a heterogeneous organocatalyst: from photochemistry to multipurpose catalysis to sustainable chemistry. *Angew. Chem. Int. Ed.* **51**, 68–89 (2012).
13. Liu, J. *et al.* Fabrication of flexible, all-reduced graphene oxide non-volatile memory devices. *Adv. Mater.* **25**, 233–238 (2013).
14. Ling, Q. *et al.* WORM-type memory device based on a conjugated copolymer containing europium complex in the main chain. *Electrochem. Solid-State Lett.* **9**, 268–272 (2006).
15. Waser, R. & Aono, M. Nanoionics-based resistive switching memories. *Nat. Mater.* **6**, 833–840 (2007).
16. Linn, E., Rosezin, R., Kügeler, C. & Waser, R. Complementary resistive switches for passive nanocrossbar memories. *Nat. Mater.* **9**, 403–406 (2010).
17. Watanabe, Y. *et al.* Current-driven insulator-conductor transition and nonvolatile memory in chromium-doped SrTiO3 single crystals. *Appl. Phys. Lett.* **78**, 3738–3740 (2001).
18. Borghetti, J. *et al.* Memristive switches enable stateful logic operations *via* material implication. *Nature* **464**, 873–876 (2010).
19. Strukov, D. B. & Likharev, K. K. A reconfigurable architecture for hybrid digital circuits with two-terminal nanodevices. *Nanotechnol.* **16**, 888 (2005).
20. Xia, Q. *et al.* Memristor-CMOS hybrid integrated circuits for reconfigurable logic. *Nano Lett.* **9**, 3640–3645 (2009).
21. Lee, S. *et al.* Resistive switching characteristics of ZnO thin film grown on stainless steel for flexible nonvolatile memory devices. *Appl. Phys. Lett.* **95**, 262113–262116 (2009).
22. Cheng, C. H., Yeh, F. S. & Chin, A. Low-power high-performance non-volatile memory on a flexible substrate with excellent endurance. *Adv. Mater.* **23**, 902–905 (2011).
23. Kim, S. & Choi, Y. K. Resistive switching of aluminum oxide for flexible memory. *Appl. Phys. Lett.* **92**, 223508–223511 (2009).
24. Jeong, H. Y., Kim, Y. I., Lee, J. Y. & Choi, S. Y. A low-temperature-grown TiO_2-based device for the flexible stacked RRAM application. *Nanotechnol.* **21**, 115203–115206 (2010).
25. Liu, J. *et al.* Preparation of MoS_2-polyvinylpyrrolidone nanocomposites for flexible nonvolatile rewritable memory devices with reduced graphene oxide electrodes. *Small* **8**, 3517–3522 (2012).
26. Yin, Z. *et al.* Synthesis of few-layer MoS_2 nanosheet-coated TiO_2 nanobelt heterostructures for enhanced photocatalytic activities. *Small* **9**, 727–730 (2012).
27. Tseng, R. J. *et al.* Polyaniline nanofiber/gold nanoparticle nonvolatile memory. *Nano Lett.* **5**, 1077–1080 (2005).
28. Wang, H. *et al.* Resistive switching characteristics of thin NiO film based flexible nonvolatile memory devices. *Microelectron. Eng.* **91**, 144–146 (2012).
29. Ji, Y. *et al.* Stable switching characteristics of organic nonvolatile memory on a bent flexible substrate. *Adv. Mater.* **22**, 3071–3075 (2010).
30. Yang, Y. C. *et al.* Fully room-temperature-fabricated nonvolatile resistive memory for ultrafast and high-density memory application. *Nano Lett.* **9**, 1636–1643 (2009).
31. Son, D. I. *et al.* Polymer-ultrathin graphite sheet-polymer composite structured flexible nonvolatile bistable organic memory devices. *Nanotechnol.* **22**, 295203–295206 (2010).
32. Huang, C. M. *et al.* Electrical bistable memory device based on a poly (styrene-b-4-vinylpyridine) nanostructured diblock copolymer thin film. *Appl. Phys. Lett.* **93**, 203303–203306 (2009).
33. Liu, J. *et al.* Bulk heterojunction polymer memory devices with reduced graphene oxide as electrodes. *ACS Nano* **4**, 3987–3992 (2010).
34. He, C. *et al.* Nonvolatile resistive switching memory based on amorphous carbon. *Appl. Phys. Lett.* **95**, 232101–232104 (2010).
35. Yi, M. *et al.* Electrical characteristics and carrier transport mechanisms of write-once-read-many-times memory elements based on graphene oxide diodes. *J. Appl. Phys.* **110**, 63709–63713 (2011).
36. Zhao, F. *et al.* Chemoselective photodeoxidization of graphene oxide using sterically hindered amines as catalyst: Synthesis and applications. *ACS Nano* **6**, 3027–3033 (2012).
37. Seo, S. *et al.* Nitrogen-Doped Partially Reduced Graphene Oxide Rewritable Nonvolatile Memory. *ACS Nano* **7**, 3607–3615 (2013).
38. Jeong, H. Y. *et al.* Graphene oxide thin films for flexible nonvolatile memory applications. *Nano Lett.* **10**, 4381–4386 (2010).
39. Novoselov, K. S. *et al.* Electric field effect in atomically thin carbon films. *Science* **306**, 666–669 (2004).
40. Berger, C. *et al.* Electronic confinement and coherence in patterned epitaxial graphene. *Science* **312**, 1191–1196 (2006).
41. Choucair, M., Thordarson, P. & Stride, J. A. Gram-scale production of graphene based on solvothermal synthesis and sonication. *Nat. Nanotechnol.* **4**, 30–33 (2008).
42. Zhang, Y. L. *et al.* Direct imprinting of microcircuits on graphene oxides film by femtosecond laser reduction. *Nano Today* **5**, 15–20 (2010).
43. Cheng, H. *et al.* Graphene Fibers with Predetermined Deformation as Moisture-Triggered Actuators and Robots. *Angew. Chem. Int. Ed.* **52**, 10482–10486 (2013).
44. ElKady, M. F., Strong, V., Dubin, S. & Kaner, R. B. Laser scribing of high-performance and flexible graphene-based electrochemical capacitors. *Science* **335**, 1326–1330 (2012).
45. Gao, W. *et al.* Direct laser writing of micro-supercapacitors on hydrated graphite oxide films. *Nat. Nanotechnol.* **6**, 496–500 (2011).
46. Yang, S. *et al.* Exfoliated graphitic carbon nitride nanosheets as efficient catalysts for hydrogen evolution under visible light. *Adv. Mater.* **25**, 2452–2456 (2013).
47. Li, J. *et al.* A facile approach to synthesize novel oxygen-doped g-C_3N_4 with superior visible-light photoreactivity. *Chem. Commun.* **48**, 12017–12019 (2012).
48. Liu, G. *et al.* Unique electronic structure induced high photoreactivity of sulfur-doped graphitic C_3N_4. *J. Am. Chem. Soc.* **132**, 11642–11648 (2011).
49. Butler, S. Z. *et al.* Progress, challenges, and opportunities in two-dimensional materials beyond graphene. *ACS Nano* **7**, 2898–2926 (2013).
50. Chen, W. & Yan, L. Centimeter-sized dried foam films of graphene: preparation, mechanical and electronic properties. *Adv. Mater.* **24**, 6229–6233 (2012).
51. Sun, G. *et al.* Preparation of weavable, all-carbon fibers for non-volatile memory devices. *Angew. Chem. Int. Ed.* **125**, 13593–13597 (2013).
52. Kim, K. S. *et al.* Large-scale pattern growth of graphene films for stretchable transparent electrodes. *Nature* **457**, 706–710 (2009).
53. Zhang, Y., Thomas, A., Antonietti, M. & Wang, X. Activation of carbon nitride solids by protonation: Morphology changes, enhanced ionic conductivity, and photoconduction experiments. *J. Am. Chem. Soc.* **131**, 50–51 (2008).
54. Xie, L. H., Ling, Q. D., Hou, X. Y. & Huang, W. An effective Friedel-Crafts postfunctionalization of poly(N-vinylcarbazole) to tune carrier transportation of supramolecular organic semiconductors based on π-stacked polymers for nonvolatile flash memory cell. *J. Am. Chem. Soc.* **130**, 2120–2121 (2008).
55. Yang, Y. *et al.* Observation of conducting filament growth in nanoscale resistive memories. *Nat. Commun.* **3**, 732–735 (2012).
56. Sze, S. M. *Physics of Semiconductor Devices* (Wiley, New York 1981).
57. Lin, Z. Q. *et al.* Spirocyclic aromatic hydrocarbon-based organic nanosheets for eco-friendly aqueous processed thin-film non-volatile memory devices. *Adv. Mater.* **25**, 3663–3666 (2013).

Acknowledgments

We thank the financial support from the 973 program of China (2011CB013000) and NSFC (21325415, 21174019, and 51161120361), Fok Ying Tong Education Foundation (no. 131043), and 111 Project 807012.

Author contributions

L.Q. and F.Z. conceived and designed the experiments. F.Z. prepared the samples and performed characterization with the assistance from H.C., Y.H. and L.S. L.Q. discussed with Z.Z. and L.J. for the experimental design and results. L.Q. and F.Z. were mainly responsible for preparing the manuscript with further inputs from other authors. All the authors discussed the results and commented on the manuscript.

Additional information

Supplementary information accompanies this paper at http://www.nature.com/scientificreports

Competing financial interests: The authors declare no competing financial interests.

How to cite this article: Zhao, F. *et al*. Functionalized Graphitic Carbon Nitride for Metal-free, Flexible and Rewritable Nonvolatile Memory Device via Direct Laser-Writing. *Sci. Rep.* **4**, 5882; DOI:10.1038/srep05882 (2014).